RSC Advances

This is an *Accepted Manuscript*, which has been through the Royal Society of Chemistry peer review process and has been accepted for publication.

Accepted Manuscripts are published online shortly after acceptance, before technical editing, formatting and proof reading. Using this free service, authors can make their results available to the community, in citable form, before we publish the edited article. This *Accepted Manuscript* will be replaced by the edited, formatted and paginated article as soon as this is available.

You can find more information about *Accepted Manuscripts* in the Information for Authors.

Please note that technical editing may introduce minor changes to the text and/or graphics, which may alter content. The journal's standard Terms & Conditions and the Ethical guidelines still apply. In no event shall the Royal Society of Chemistry be held responsible for any errors or omissions in this *Accepted Manuscript* or any consequences arising from the use of any information it contains.

ROYAL SOCIETY OF CHEMISTRY

www.rsc.org/advances

Low temperature Au induced crystallization of Titanium dioxide thin films for Resistive switching applications

L.D. Varma Sangani[a], K. Vijaya Sri[a], Md. Ahamad Mohiddon[b,]*, M. Ghanashyam Krishna[a,b]
[a]Centre for Advanced Studies in Electronics Science and Technology, School of Physics,
[b]School of Physics, University of Hyderabad, Hyderabad 500046, Telangana, India
Phone : (+) 91-40-23134382, FAX: (+) 91-40-23010227, Email: ahamed.vza@gmail.com

Abstract

Metal induced decrease of crystallization temperature of sol-gel derived titanium dioxide (TiO_2) thin films is reported. It is shown that the Au induced onset of crystallization occurs at a temperature of 250^{o}C as compared to 400^{o}C when it is deposited directly on the same substrate. The crystallization process is probed using x-ray diffraction and confirmed by Raman spectroscopy. The onset of crystallization is evidenced by the appearance of the diffraction peak from the (101) plane of anatase TiO_2 and the peak due to A_{1g} + B_{1g} Raman mode at 515 cm^{-1}. Polarized optical microscopy and Raman imaging indicated that the spatial spread of crystallization across the surface of the film increases with increase in temperature. Unipolar Resistive switching is demonstrated by fabricating an Au/TiO_2/Au stack, which shows formation at 9V, set voltage of 0.5V and reset voltage of 3.3V. The maximum set-reset resistance ratio achieved was 10^5. The mechanism of resistive switching is established by a correlation with photoluminescence spectra which indicate the presence of defects that aid in the switching process.

Keywords: Titania, metal induced crystallization, Resistive switching, photoluminescence

1. Introduction

Low temperature (*i.e.* temperatures < 400^{o}C) crystallization of oxide thin films grown by chemical solution techniques is essential, since many electronic and optoelectronic devices are fabricated on substrates that cannot withstand high temperatures. For example, decrease in crystallization temperatures of amorphous Silicon films has been achieved by techniques including excimer laser annealing,[1] metal-induced crystallization (MIC)[2] and electric field-aided crystallization.[3] In MIC, a thin layer of metal such as Ni, Cr, Al, Au or Sn is brought in contact with the amorphous Si film. This results in the reduction of the crystallization

RSC Advances Accepted Manuscript

temperature as a result of silicide seeding or layer excahnge.[4] The driving force behind metal induced crystallization is the difference in the free energy between amorphous and crystalline phases of the material.[5] Titanium dioxide (titania) has been one of the most prominent oxide materials for many years due to its application in diverse fields.[6–10] More recently, there has been a resurgence of interest in TiO_2 because of its resistive switching behavior and is one of the main contenders for next-generation non-volatile memory devices.[11,12] In spite of the fact that the MIC process is well studied for amorphous silicon and the mechanism behind its crystallization is understood, there are very few reports of such studies in the case of oxide films.[13–16]Yang et al. have reported that Cu and Ni induced crystallization reduces the crystallization temperature by 30^{o}C (from ~250 to ~220^{o}C).[15] Sarrano et al. have reported that the anatase to rutile phase transformation occurs at relatively lower temperatures in Ag doped Titania films.[17] Perkas et al. have reported gold induced crystallization of SiO_2 and TiO_2 powders at 80^{o}C by insertion of Au nanoparticles.[18] Clearly, there is evidence that metal induced crystallization can aid in lowering the crystallization temperature of TiO_2. However, there are no reports of such studies on sol-gel derived TiO_2 films. Low temperature synthesis of TiO_2 films is important in the context of electronic and opto-electronic applications since it will enhance the possibility of fabricating such devices on substrates such as glass. The objectives of the present study are, therefore, to demonstrate (1) Au induced low temperature crystallization of sol-gel derived TiO_2 thin films and (2) resistive switching in an Au/TiO_2/Au memory device. X-ray diffraction, Raman spectroscopy, polarized light optical microscopy, Raman imaging and Photoluminescence (PL) have been used to confirm the crystallization of TiO_2.

2. Experimental

Au films of 80nm thickness were deposited on a borosilicate glass (BSG) substrate by ion beam sputter deposition. The details of the Au film deposition are discussed elsewhere.[19] TiO_2 sols were synthesized by the hydrolysis of alkoxides in alcoholic solutions in the presence of an acid catalyst. The procedure of preparation includes the dissolution of one mole of tetrabutyl-orthotitanate ($(C_4H_9O)_4Ti$ or TTiP (Aldrich Chemicals) in four moles of acetic acid (CH_3COOH). One mole each of distilled water and Ethanol (C_2H_5OH) are added as solvents. This solution is transparent and ready for thin film deposition. The BSG substrates were ultrasonically cleaned in acetone and methanol, followed by rinsing in iso-propanol and drying in a vacuum oven. The TiO_2 thin films were spin coated (Spin 150-NPP)

RSC Advances Accepted Manuscript

at 3000 rpm, from the resulting sol, on the BSG substrates. The thickness of the films was measured after deposition using a surface profilometer (model XP-1 of Ambios Technology, USA). A series of BSG/TiO_2 and BSG/Au/TiO_2 stacks were heated to temperatures ranging from 200 to 500^oC for 4hr in ambient atmosphere. The extent of TiO_2 crystallization was followed in a powder x-ray diffractometer (CPS120 of Inel, France) equipped with a Co Kα X-ray source (wavelength = 0.178896 nm) and gas phase position sensitive detector. The Raman spectra were recorded in air using an Nd-YAG 532 nm laser in the back scattering geometry (model alpha 300 of WiTec, Germany). Polarized light confocal optical microscopy (POM) images were acquired at room temperature to probe the crystallization of TiO_2 with annealing temperature. Plane polarized 532nm laser is focused by 100× objectives on to the sample and the reflected signal is collected through cross Polaroid configuration and sent to photomultiplier tube (PMT) detector. 500×500 points were chosen across the selected region over each sample. The laser power is maintained such that the PMT detector remains unsaturated. The surface features of the samples were imaged in a field emission scanning electron microscope (FE-SEM Model Ultra55 of Carl Zeiss, Germany). The photoluminescence (PL) spectra are collected in backscattering mode on 355nm diode laser excitation source based PL spectrometer (WiTec alpha 300 SNOM instrument) operated at 7 mW. The Au/TiO_2/Au resistive random access memory (RAM) device was fabricated by thermal evaporation and spin coating techniques. In brief, 80nm Au bottom electrode was deposited on BSG substrate by thermal evaporation. This is followed by the deposition and annealing of a 100nm thick TiO_2 film, as discussed above. Top electrodes of Au of 1mm diameter were coated using shadow mask technique by thermal evaporation. The schematic representation of fabricated resistive RAM device is presented in the Fig. 1. Resistive RAM characterizations are carried out in a semiconductor device analyzer (Agilent B1500).

3. Results and Discussion

The sol-gel derived TiO_2 thin films deposited directly on BSG substrates (referred as BT films in the rest of the paper) are transparent whereas the BSG/Au/TiO_2 thin film stacks (referred as BAT films in the rest of the paper) are opaque due to the thin gold under-layer. The effect of annealing temperature on the crystallization of BT thin films is presented using X-ray diffraction and Raman spectroscopy in Fig. 2(a) and (b), respectively. The X-ray diffraction pattern of BT thin films displayed in Fig. 2(a) demonstrates that the crystallization is initiated at 400^oC. The XRD pattern of TiO_2 thin films annealed up to 300^oC has a broad

RSC Advances Accepted Manuscript

peak centered on 2θ=26.5°, which may be assigned to the amorphous BSG substrate. At higher annealing temperature of 400°C, a strong broad peak centered on 2θ = 29.4° which may be assigned to the (101) plane of anatase phase of TiO_2 appeared. Additional faint peaks at 2θ = 36.9° and 56.5° are also indentified as belonging to the (110) and (200) planes of anatase phase of TiO_2 (indexed according to the PCPDF file no- 89-4203). The intensity of the peaks increases with increase in annealing temperature to 500°C. From this study, it is observed that the onset of crystallization of the BT thin film in to the anatase phase occurs at 400°C. The crystallite sizes of the samples annealed at different temperatures were derived from the full width half maxima of the intense (101) peak using Debye-Scherrer relation.[20] The calculated crystallite size is approximately same for samples annealed at 400 and 500°C, i.e. 9±2 nm. The modification of titanium alkoxide by chemical reaction, formation of intermediate complex ligands and the subsequent formation of TiO_2 nanoparticles using Raman and IR spectroscopy techniques are commonly reported in the literature.[21] The Raman scattering spectra excited by 532nm Nd-YAG laser, for BT thin films annealed at various temperatures is displayed in Fig. 2(b). The Raman spectra for the BT films annealed at 200 and 300°C have a strong and broad band around 560 cm^{-1}, along with weak bands at 456 and 670 cm^{-1}, which may be assigned to the intermediate ligand complex.[22] This observation leads to the inference that the titanium alkoxide did not result in the formation of Titania up to an annealing temperature of 300°C. However, the spectrum for the film annealed at 400°C exhibited a dramatic change with the appearance of a new Raman band centered around 635 cm^{-1}. Significantly, there is a complete absence of the previously observed Raman bands indicating that the intermediate ligand complex has decomposed to form Titania at 400°C. The intensity of the band centered around 635cm^{-1} is strengthened for the film annealed at 500°C, indicating the relatively enhanced TiO_2 crystallization. This Raman band at 635cm^{-1} can be assigned to the E_g mode of the anatase phase of TiO_2. The anatase phase of TiO_2 has six allowed modes ($A_{1g} + 2B_{1g} + 3E_g$)[23] at 143.4 cm^{-1} (E_g),196.2 cm^{-1} (E_g), 396.5 cm^{-1} (B_{1g}), 517.7 cm^{-1} ($A_{1g} + B_{1g}$), and 639.4 cm^{-1}(E_g).[21,23] The strong Raman band centered around 635 cm^{-1} in BT films annealed at 500°C confirm that the TiO_2 films crystallized in to the anatase phase. The shift in the peak position (~635cm^{-1}) and broad peak width (~60cm^{-1}) of the Raman band of anatase TiO_2 E_g mode may be due to the particle size effect (9±2 nm). The phonon confinement model or spatial correlation model explains the correlation between particle size and phonon momentum distribution.[24,25] Phonons are increasingly confined within the particle with reduction in particle size and hence the distribution of phonon

RSC Advances Accepted Manuscript

momentum increases. This phonon dispersion causes asymmetric broadening and may lead to a shift of the Raman bands.[24,25] From a detailed study of XRD and Raman spectra, it is concluded that the onset of crystallization of BT thin films occurs at 400^{o}C.

The X-ray diffraction patterns and Raman spectra of the BAT films annealed at various temperatures from 250^{o}C to 450^{o}C for 4hr are compared in Fig. 3 and Fig. 4 respectively. The XRD pattern of BAT films annealed at different temperatures have a set of strong diffraction peaks (shown in Fig 3(a)) which are identified as belonging to the thin Au layer. There is a weak diffraction peak at 2θ =30.9^{o} distinctly visible in the magnified XRD pattern in the range of 2θ= 28 to 34^{o} in Fig. 3(b). The intensity of this peak continues to increase with increase in annealing temperature and it can be assigned to the (101) plane of the anatase phase indicating onset of TiO_2 crystallization at 250^{o}C. Further, the BAT stack annealed at 400^{o}C has an additional low intensity peak at 2θ =56.9^{o} which can be assigned to the (200) plane of anatase TiO_2. From this observation, it is inferred that the TiO_2 crystallization is initiated at 250^{o}C. This is in contrast to the BT films, wherein it was observed that onset of crystallization occurs at 400^{o}C. Hence, the introduction of a Au metal layer decreases the crystallization temperature by almost 150^{o}C. The crystallite size calculated from FWHM of (101) plane is 13±3nm for the BAT films annealed from 250 to 450^{o}C. No systematic change in the crystallite size is observed with annealing temperature. However, the size of crystallites is relatively larger in the case of BAT samples as compared to the BT samples. Similar observation of relatively long range crystallization is reported for Al/Sn induced Silicon crystallization. [20,26] The Raman spectra of BAT films annealed at different temperatures presented in Fig. 4(a) also confirms the argument drawn from XRD results. The Raman spectra of the BAT film annealed at 250^{o}C (shown in Fig. 4(b)) has a diffuse and broad feature at 515 and 639 cm^{-1}, which may belong to the TiO_2 anatase phase. A relatively distinct and broad Raman peak centered around 639 cm^{-1} is recorded for the BAT films annealed at 300^{o}C. With further increase in annealing temperature, the Raman modes of anatase phase of TiO_2 at 391(B_{1g}), 515 cm^{-1} (A_{1g} + B_{1g}) and 639.4 cm^{-1}(E_g) become more intense. The increase in the intensity and decrease in the full width at half maxima of these three Raman modes with annealing temperatures indicates the increase in the crystallization of anatase phase of TiO_2. A small shift in Raman modes for the sample annealed at 250^{o}C can be attributed to the onset of crystallization and small particle dimensions. Further confirmation of TiO_2 crystallization is derived from confocal POM micrographs depicted in Fig. 5 (a)-(d) for the BAT stacks annealed at a) 250, b) 300, c)350

RSC Advances Accepted Manuscript

and d) 400°C. The POM image of BAT stacks annealed at 250°C shows initiation of crystallization centers that are very small in dimension. At 300°C, there is growth of these crystal centers which are distributed across the surface of the sample with approximate dimensions in the range of 500 nm to 1 μm. The dimensions of the crystallized regions are found to increase with annealing temperatures at 350°C and 400°C respectively. This observation supports the inference drawn from XRD and Raman spectroscopy that the presence of Au induced lower temperature crystallization of the TiO_2 films. To further investigate the two regions identified in POM, Raman imaging technique has been employed to investigate the nature of crystallization across the surface of the sample. A 25×25 μm^2 region was subjected to Raman imaging and 100×100 Raman spectra with spectral integration time of 3s were collected. The Raman image was extracted by selecting a filter across the Raman shift of 639 cm^{-1}, which is the E_g mode of anatase TiO_2 phase. The Raman images of annealed BAT films are shown in Fig. 6(a)-(d) for temperatures of (a) 250°C, (b) 350°C ,(c) 400°C and (d) 450°C. The Raman image of BAT film sintered at 450°C extracted for the Raman shift at 0 cm^{-1} is presented in the Fig. 6(e). The Raman spectra of BAT film annealed at 250°C has circular bright regions of diameter approximately 2μm. The brightness of the circular region is proportional to the area under the Raman shift centered at 639 cm^{-1}, which further indicates the extent of TiO_2 crystallization. However, there are relatively less bright regions of the order of same dimension distributed across the Raman image which correspond to lower intensity of E_g mode peak. In contrast, the completely dark regions belong to amorphous part of the BAT film. For confirmation of this inference, the Raman spectra collected in dark and bright regions of the BAT film are presented in the Fig. 6(f). The dimensions and distribution of the bright regions increases with annealing temperature, which further confirms the inferences drawn from the XRD and Raman studies, discussed earlier. It was observed that the dimensions of crystallized regions obtained in POM and Raman imaging are slightly different. This is due to difference in the resolution and number of points collected across the unit region. Further, to verify that the Raman image is not influenced by artefacts in the morphology of the sample, the Raman image for the Raman shift centered at 0 cm^{-1} (i.e. Rayleigh scattering) for the BAT film annealed at 450°C was also extracted. It was indeed found that Rayleigh scattering is independent of the TiO_2 phase present across the surface of the sample. However, the morphology of the sample may influence the Rayleigh scattering signal, due to fluctuations in the focusing point. The Rayleigh line Raman image of the BAT sample annealed at 450°C has no feature similar to

RSC Advances Accepted Manuscript

those observed in Fig. 6(d) for the Raman shift at 639 cm^{-1} for the same sample. From this observation, we confirm that the bright regions observed in Raman images Fig. 6(a)-(d) are purely due to TiO_2 crystallized region.

These observations indicate that the mechanism of Au induced TiO_2 crystallization is similar to MIC in Au/Si[27] and Ni/TiO_2[15] bilayer systems. In the Au/Si system crystallization of a-Si is initiated when Au intermixes with the Si. Au induces instability in the bonding character of the Si adjacent to the metal by screening the coulomb interactions by its mobile free electrons. This results in the reduction of activation energy for Si dissociation at the Au/Si interface which in turn leads to the release of Si atoms that migrate readily. These free Si atoms diffuse to interfaces of the intermixed region and get crystallized[27]. An analogous mechanism has been proposed by Yang et al. for Ni induced TiO_2 crystallization, where at first the valence electrons of Ni are partially transferred to the anti-bonding orbital of Ti-O bonds in a-TiO_2 to form a O-Ti-O-Ni network[15]. In the next stage, the annealing process breaks the weakened Ti-O bonds and activates the rearrangement of Ti-O bonds leading to the crystallization of TiO_2. It is, therefore, postulated in the present case that the free electrons from Au are transferred to the adjacent Ti-O bond in TiO_2. This process weakens the Ti-O bonds and further annealing process results in rearrangement of Ti-O bonds which leads to TiO_2 crystallization.

Before proceeding to device fabrication, the surface morphology of BAT samples were examined under FESEM and are presented in the Fig. 7 (a)-(d) for annealing temperatures of a) 300, b) 350, c) 400 and d) 450^oC. A crack free, smooth and homogeneously spread morphology is observed throughout whole sample for all BAT films. Very tiny regions (grains) of few tens of nanometer with different contrast from its background, that are homogeneously distributed over the BAT film annealed at 300^oC is recorded and is shown in Fig. 7(a). The dimensions of these grains are found to increase with increase in annealing temperature in Fig. 7(b)-(d). The morphology of BAT film annealed at 450^oC in Fig. 7(d) shows, the growth of very fine pores across the intersection regions of the grains. The current-voltage (I-V) and resistance-voltage (R-V) characteristic of an Au/TiO_2/Au structure based on the BAT stack annealed at 300^oC is presented in Fig. 8(a) and 8(b), respectively. The inset in Fig. 8(a) shows that, as the voltage of positive polarity increases a sudden change in resistance was observed at 9.1 V and the resistance dropped to 10 Ω from a value of 10^9Ω (Fig. 8(b)). This voltage is called the formation voltage. The observed switching behavior is typical for a unipolar Resistive RAM device. A compliance

RSC Advances Accepted Manuscript

current of 10mA was set to avoid permanent breakdown of the device due to high current when it switched into the low resistance state. The device is reset, i.e. switch back from low resistance state (LRS) to high resistance state (HRS) at a positive voltage of 0.5 V and current of 44 mA. The reverse switching from HRS to LRS called set, was obtained at 3.3 V. This switching behavior is reproducible for a large number of cycles. The LRS and HRS resistance values are 10 Ω and 1 MΩ (from Fig. 8(b)) leading to a HRS to LRS resistance ratio of five orders. These values are comparable to those reported in literature.[28]

To determine the mechanism of switching in these films photoluminescence (PL) spectra were recorded, since they are very sensitive to the presence of defects. The PL spectra of BAT films annealed at various temperatures, for the excitation wavelength of 355nm and collected at ambient room temperature are presented in the Fig. 8(c). The electronic band structure of TiO_2 possesses a highly ionic lattice with the valence band composed of oxygen 2p orbital and the conduction band consists mostly of excited states of Ti^{4+}. It has been reported earlier[29] that there is an excitation peak at 380nm for a polycrystalline TiO_2 due to an $O^{2-} \rightarrow Ti^{4+}$charge-transfer transition within a regular titanate octahedron. In general, the PL spectra of TiO_2 have contributions from (1) exciton emission, which is due to the transitions of electrons from the conduction band to the valence band and (2) the transition of electrons from the defect energy level to the valence band. From electronic band structure calculations exciton emission is expected to lie in the wavelength range of 380-390 nm, located in the UV region, while the defect energy levels lie in the wavelength range between 400-600 nm located in the visible region.[30,31] The BAT stack annealed at 250^{o}C has no significant PL emission. In contrast, a diffuse broad emission was recorded for the film annealed at 300^{o}C. The intensity of the PL emission spectra and different contributions to the emission peak are well resolved with increase in annealing temperature. The BAT stack annealed from 300^{o}C to 450^{o}C has emission peaks at 422, 434, 468 and 515nm. The emission at 422nm can be assigned to the Wannier-Mott free excition emission, which predominates in semiconductors. Wannier-Mott excitons are described as electron-hole pairs that are free to hop between different crystal sites by exceeding the strength of their Coulomb coupling. Due to this reason, Wannier-Mott excitons possess relatively lower binding energy and hence the emission in our case (422nm) is red shifted relative to electron band structure calculations (388nm). Similar observation of Wannier-Mott excitons emission at 412 nm[32], 418nm[33] for titania has been reported earlier by other workers. The emission at 434 nm is situated at about ~650 cm^{-1} which is lower in energy to exciton emission. This shift is in good agreement with

RSC Advances Accepted Manuscript

the phonon shift of ~640 cm^{-1} for E_g mode.[21] Therefore this emission is attributed to the phonon repetition of free excition line. Similar phonon repetition emission line has been reported by Hart et al.[32] The emissions at 468nm and 515nm are assigned to the emissions due to oxygen vacancy-defect energy level transfer. Two kind of oxygen vacancies exists in titania, one is the neutral oxygen vacancy which emits at 465nm and the other is an oxygen vacancy losing an electron which emits at 515nm [31,34]. In general, the defect energy emission will dominate over the exciton emission and will strongly depend on a number of processing parameters. It can, thus, be inferred from the PL spectra that the titania films in the present case have a large number of defect states which provide the flexibility to tailor the switching properties as desired. Thus, the combination of low temperature crystallization and favorable switching properties makes the approach used in the current study very attractive for applications.

4. Conclusions

The lowering of crystallization temperature of Titania film by contact with Au layer is reported. The BSG/TiO_2 films are crystallized at temperature starting from 400^oC, in contrast to TiO_2 deposited on an Au coated BSG substrate which showed an onset of crystallization at 250^oC. Thus, we conclude from our work that the thin Au layer has brought down the crystallization temperature of Titania film by 150^oC. The crystallized BSG/Au/TiO_2 exhibit good resistive switching and photoluminescence characteristics which are suitable for technological applications.

Acknowledgements

Authors acknowledge the facilities provided by by Centre for Nanotechnology and school of Physics, University of Hyderabad, India under the UGC-CAS, UPE programs. Dr. Md. Ahamad Mohiddon acknowledges DST-SERB for the project SB/FTP/PS049/2014 and L.D. Varma Sangani acknowledges UGC-BSR fellowship of University of Hyderabad for the financial assistantship during this work.

RSC Advances Accepted Manuscript

References

1 O. Van Overschelde, R. Snyders and M. Wautelet, *Appl. Surf. Sci.*, 2007, **254**, 971–974.

2 M. A. Mohiddon, K. L. Naidu, M. G. Krishna, G. Dalba and F. Rocca, *J. Nanoparticle Res.*, 2011, **13**, 5999–6004.

3 A. Gaur and V. M. Sglavo, *J. Eur. Ceram. Soc.*, 2014, **34**, 2391–2400.

4 W. Knaepen, C. Detavernier, R. L. Van Meirhaeghe, J. J. Sweet and C. Lavoie, 2008, **516**, 4946–4952.

5 O. Nast and A. J. Hartmann, *J. Appl. Phys.*, 2000, **88**, 716.

6 W. Wang, B. Gu, L. Liang, W. a Hamilton and D. J. Wesolowski, *J. Phys. Chem. B*, 2004, **108**, 2–5.

7 A. Fujishima, T. N. Rao and D. A. Tryk, *J. Photochem. Photobiol. C Photochem. Rev.*, 2000, **1**, 1–21.

8 G. K. Mor, O. K. Varghese, M. Paulose, K. Shankar and C. A. Grimes, *Sol. Energy Mater. Sol. Cells*, 2006, **90**, 2011–2075.

9 A. L. Linsebigler, A. L. Linsebigler, J. T. Yates Jr, G. Lu, G. Lu and J. T. Yates, *Chem. Rev.*, 1995, **95**, 735–758.

10 U. Diebold, *Surf. Sci. Rep.*, 2003, **48**, 53–229.

11 C. Brinker and G. Scherer, *The physics and chemistry of sol-gel processing*, Academic Press, INC. Boston San Diego New York, 1990.

12 H. Schroeder and D. S. Jeong, *Microelectron. Eng.*, 2007, **84**, 1982–1985.

13 M. A. Mohiddon and M. G. Krishna, *J. Mater. Sci.*, 2011, **46**, 2672–2677.

14 M. Ahamad Mohiddon and M. Ghanashyam Krishna, *J. Vac. Sci. Technol. B*, 2012, **30**, 061203 1–8.

15 C. Yang, Y. Hirose, S. Nakao, N. L. H. Hoang and T. Hasegawa, *Appl. Phys. Lett.*, 2012, **101**, 52101–5.

16 C. Yang, Y. Hirose, S. Nakao and T. Hasegawa, *Thin Solid Films*, 2014, **553**, 17–20.

17 J. García-Serrano, E. Gómez-Hernández, M. Ocampo-Fernández and U. Pal, *Curr. Appl. Phys.*, 2009, **9**, 1097–1105.

18 N. Perkas, V. G. Pol, S. V. Pol and A. Gedanken, 2006, **6**, 293–96.

RSC Advances Accepted Manuscript

19 R. Brahma, G. M. Reddy, P. A. Lakshmi, S. Singh and M. G. Krishna, *J. Nanosci. Nanotechnol.*, 2011, **11**, 6843–6851.

20 M. A. Mohiddon and M. G. Krishna, *J. Mater. Sci.*, 2012, **47**, 6972–6978.

21 M. C. Mathpal, A. K. Tripathi, M. K. Singh, S. P. Gairola, S. N. Pandey and A. Agarwal, *Chem. Phys. Lett.*, 2013, **555**, 182–186.

22 I. Karatchevtseva, D. J. Cassidy, Z. Zhang, G. Triani, K. S. Finnie, S. L. Cram, C. J. Barbé and J. R. Bartlett, *J. Am. Ceram. Soc.*, 2008, **91**, 2015–2023.

23 T. Ohsaka, *J. Phys. Soc. Japan*, 1980, **48**, 1661–1668.

24 W. S. Li, Z. X. Shen, H. Y. Li, D. Z. Shen and X. W. Fan, *J. Raman Spectrosc.*, 2001, **32**, 862–865.

25 H. C. Choi, Y. M. Jung and S. Bin Kim, *Vib. Spectrosc.*, 2005, **37**, 33–38.

26 O. Nast and A. J. Hartmann, 2000, **88**, 716–724.

27 P. A. P. L Hulman, A. Robertsson, T.G. Hentzell, I. Engstrom, *J. Appl. Phys.*, 1987.

28 B. J. Choi, S. Choi, K. M. Kim, Y. C. Shin, C. S. Hwang, S. Y. Hwang, S. S. Cho, S. Park and S. K. Hong, *Appl. Phys. Lett.*, 2006, **89**, 012906 1–3.

29 S. K. Deb, *Solid State Commun.*, 1972, **11**, 713–715.

30 D. Li, N. Ohashi, S. Hishita, T. Kolodiazhnyi and H. Haneda, *J. Solid State Chem.*, 2005, **178**, 3293–3302.

31 D. Fang, K. Huang, S. Liu and J. Huang, *J. Braz. Chem. Soc.*, 2008, **19**, 1059–1064.

32 L. G. J. de Haart and G. Blasse, *J. Solid State Chem.*, 1986, **61**, 135–136.

33 Y. Zhu and C. Ding, *J. Solid State Chem.*, 1998, **127**, 124–127.

34 Y. H. Chang, C. M. Liu, C. Chen and H. E. Cheng, *J. Electrochem. Soc.*, 2012, **159**, D401–D405.

RSC Advances Accepted Manuscript

Bibliography

Mr. L D Varma Sangani has received his bachelor degree in engineering from Sagi Rama Krishnam Raju Engineering College, Andhra University in 2009. Currently, He is pursuing his PhD in University of Hyderabad, India and his area of interest includes fabrication and characterization of Resistive Random Access Memory and Electron Beam Lithography.

Mrs. Vijaya Sri has received her bachelor degree in engineering from Sir Cattamanchi Ramalinga Reddy College of Engineering, Andhra University in 2012 and master degree in engineering from University of Hyderabad in 2014. Her research interest includes growth and characterization of thin films and device fabrication for Resistive Random Access Memory applications.

Dr. Md Ahamad Mohiddon has received his PhD in Physics, 2009 from Indian Institute of Technology Roorkee. He was a postdoctoral fellow at University of Trento, Italy and currently, He is a DST-Young Scientist at School of Physics - Central facility for Nanotechnology, University of Hyderabad, India. His research interest includes Metal Induced Crystallization, metal/semi conductor interfaces and engineering of plasmonic field strength over metal/dielectric superstructures by near field optical microscopy for application in surface enhanced Raman scattering.

Dr. M Ghanashyam Krishna received his Bachelor's and Master's degrees from University of Delhi and PhD from Indian Institute of Science, Bangalore, India in 1992 in the area of oxide thin films. After a post doctoral stint at the University of Warwick, UK, Ghanashyam Krishna joined the faculty of the School of Physics, University of Hyderabad in 2001 where he has been a Professor since 2010. His research interests include electronic, optical, optoelectronic and sensing applications of nanostructured thin films.

RSC Advances Accepted Manuscript

Figure captions:

Figure 1: Schematic representation of Au/TiO_2/Au resistive RAM memory device.

Figure 2: (a) X-ray diffraction pattern and (b) Raman spectra of BSG/TiO_2 (BT) films annealed at different temperatures.

Figure 3: (a) X-ray diffraction pattern along with (b) the magnified 2θ region for BSG/Au/TiO_2 (BAT) films annealed at different temperatures.

Figure 4: (a) Raman spectra of BSG/Au/TiO_2 (BAT) films annealed at different temperatures along with (b) magnified Raman spectra of BAT film annealed at 250^{o}C.

Figure 5: Polarized light confocal optical micrographs of BSG/Au/TiO_2 (BAT) films annealed at (a) 250^{o}C, (b) 300^{o}C, (c) 350^{o}C and (d) 400^{o}C.

Figure 6: Raman image extracted for the E_g Raman mode at 639cm^{-1} for BAT films annealed at (a) 250^{o}C, (b) 350^{o}C, (c) 400^{o}C, (d) 450^{o}C, (e) Rayleigh line (0 cm^{-1}) Raman image of BAT film annealed at 450^{o}C, (f) Raman spectra collected in the bright and dark region of the Raman images (a)-(d)

Figure 7: Field emission scanning electron micrographs of BSG/Au/TiO_2 (BAT) films annealed at (a) 300^{o}C, (b) 350^{o}C, (c) 400^{o}C and (d) 450^{o}C.

Figure 8: (a) Current-Voltage and (b) Resistive-Voltage characteristics of Au/TiO_2/Au resistive RAM device fabricated at 300^{o}C; (c) Photoluminescence spectra of BSG/Au/TiO_2 (BAT) films annealed at different temperatures.

RSC Advances Accepted Manuscript

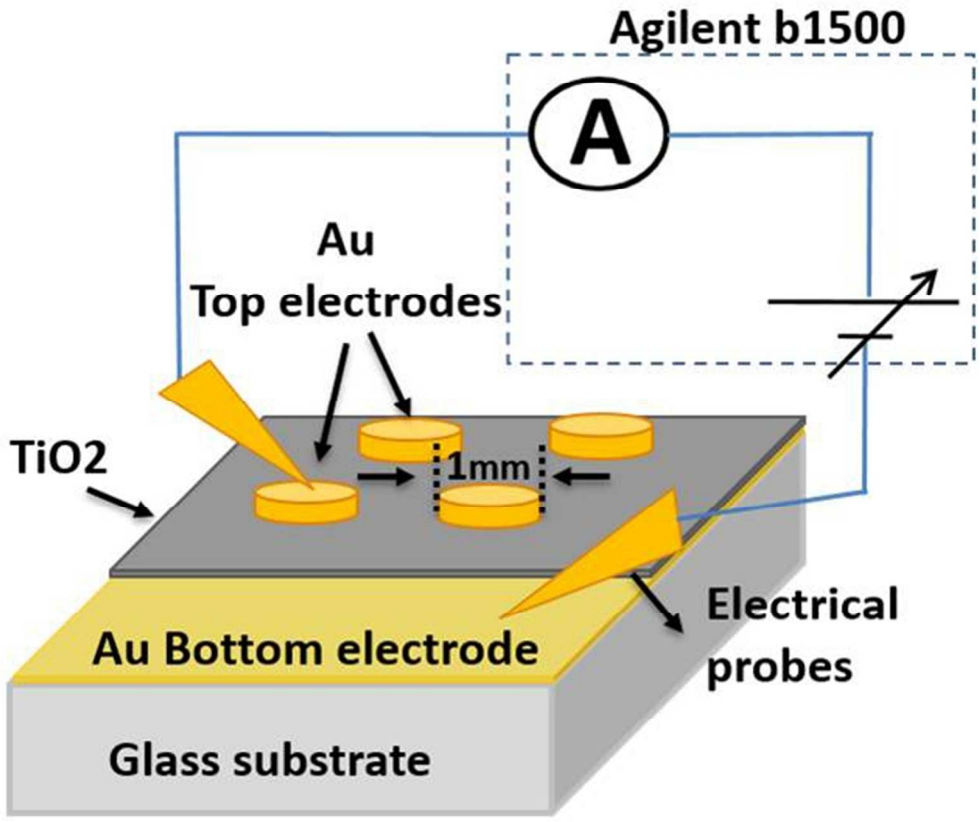

Schematic representation of Au/TiO2/Au resistive RAM memory device.
177x150mm (92 x 92 DPI)

RSC Advances Accepted Manuscript

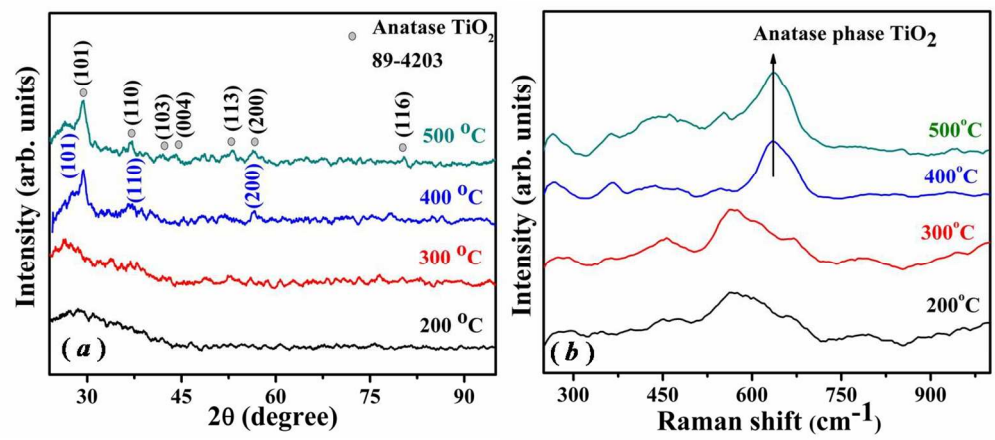

(a) X-ray diffraction pattern and (b) Raman spectra of BSG/TiO2 (BT) films annealed at different temperatures.
251x112mm (150 x 150 DPI)

RSC Advances Accepted Manuscript

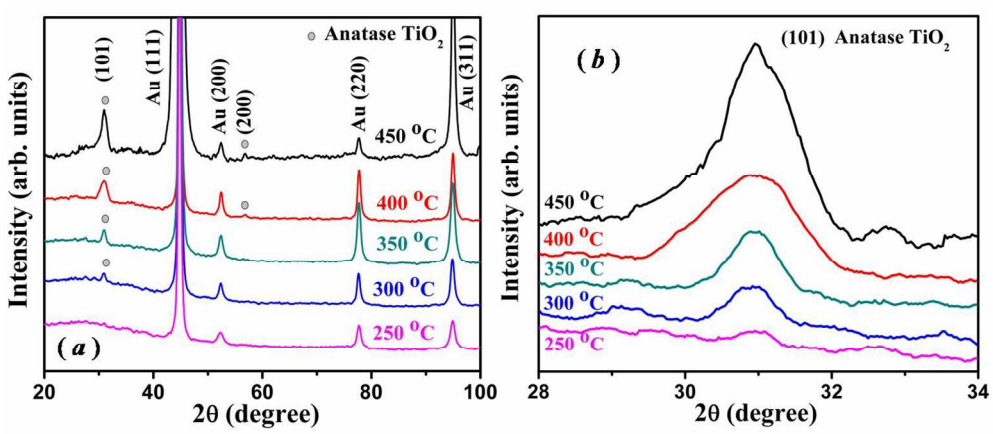

(a) X-ray diffraction pattern along with (b) the magnified 2θ region for BSG/Au/TiO2 (BAT) films annealed at different temperatures.
259x112mm (150 x 150 DPI)

RSC Advances Accepted Manuscript

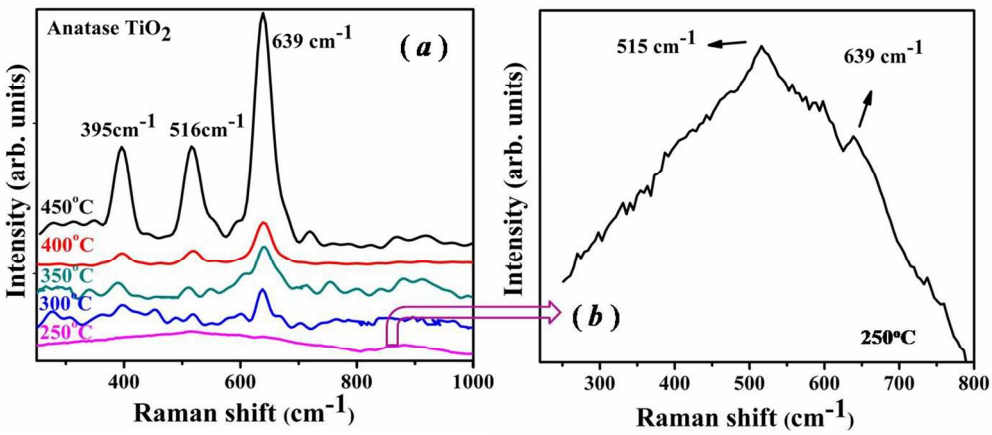

(a) Raman spectra of BSG/Au/TiO2 (BAT) films annealed at different temperatures along with (b) magnified Raman spectra of BAT film annealed at 250oC
234x102mm (150 x 150 DPI)

RSC Advances Accepted Manuscript

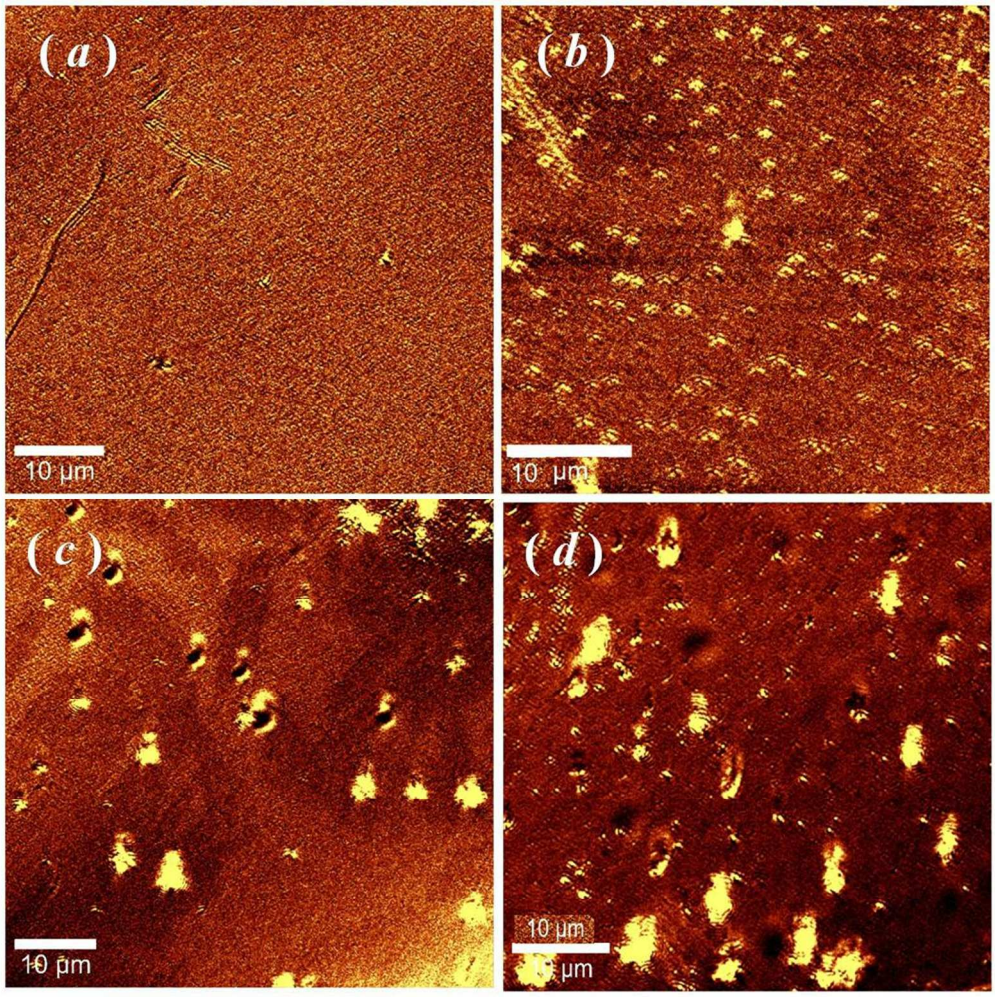

Polarized light confocal optical micrographs of BSG/Au/TiO2 (BAT) films annealed at (a) 250oC, (b) 300oC, (c) 350oC and (d) 400oC.
178x178mm (150 x 150 DPI)

RSC Advances Accepted Manuscript

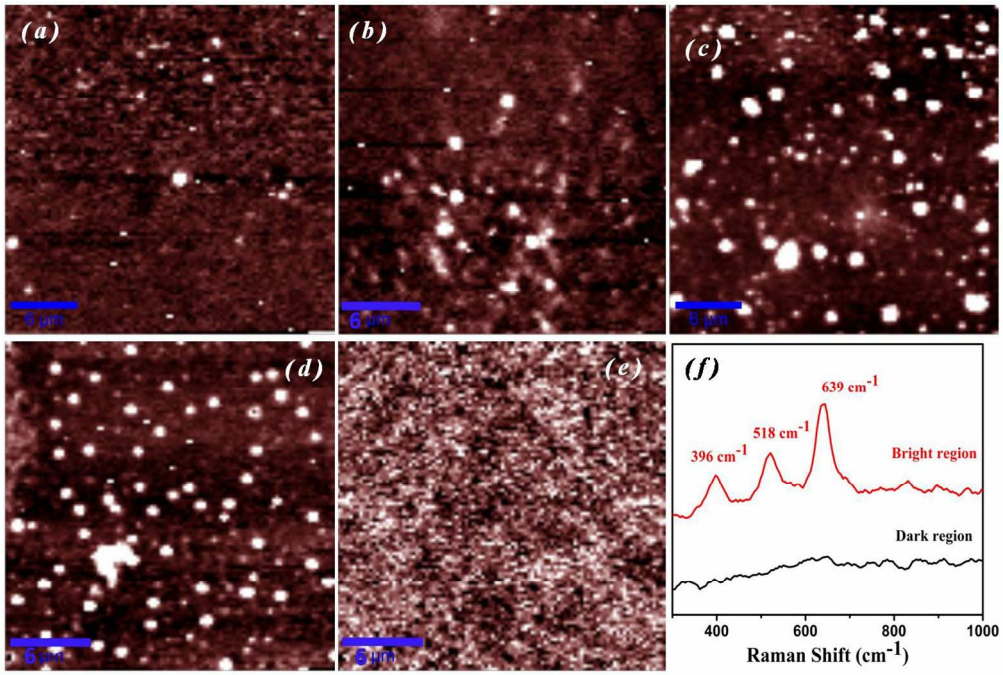

Raman image extracted for the Eg Raman mode at 639cm-1 for BAT films annealed at (a) 250oC, (b) 350oC, (c) 400oC, (d) 450oC, (e) Rayleigh line (0 cm-1) Raman image of BAT film annealed at 450oC, (f) Raman spectra collected in the bright and dark region of the Raman images (a)-(d)
265x178mm (150 x 150 DPI)

RSC Advances Accepted Manuscript

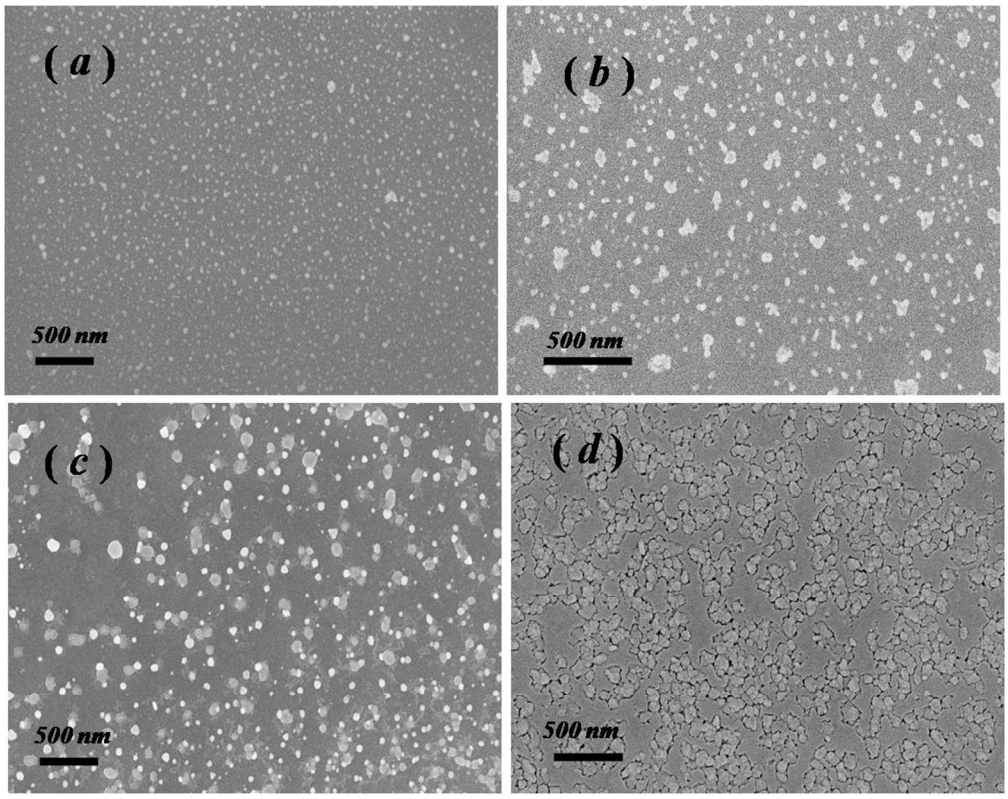

Field emission scanning electron micrographs of BSG/Au/TiO2 (BAT) films annealed at (a) 300oC, (b) 350oC, (c) 400oC and (d) 450oC.
195x154mm (150 x 150 DPI)

RSC Advances Accepted Manuscript

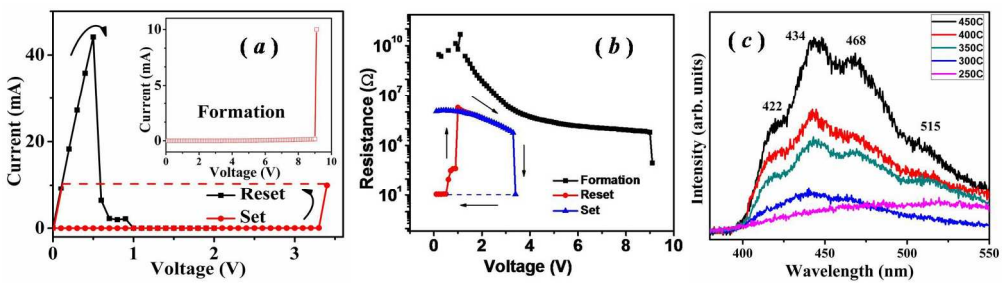

(a) Current-Voltage and (b) Resistive-Voltage characteristics of Au/TiO2/Au resistive RAM device fabricated at 300oC; (c) Photoluminescence spectra of BSG/Au/TiO2 (BAT) films annealed at different temperatures.
365x101mm (150 x 150 DPI)

RSC Advances Accepted Manuscript